J. Fluid Mech. (1989), *vol.* 205, *pp.* 297–318
Printed in Great Britain

Turbulent dynamos driven by convection

By M. MENEGUZZI[1] AND A. POUQUET[2]

[1]CERFACS, 42 avenue Coriolis, 31000 Toulouse *and* Service d'Astrophysique, Centre d'Etudes Nucléaires de Saclay, France

[2]High Altitude Observatory, NCAR, Boulder, CO 80307, USA *and* LA 128, CNRS, Observatoire de Nice, BP 139, 06007 Nice, France

(Received 21 April 1987 and in revised form 11 February 1989)

The generation of magnetic fields by the turbulent motions of a conducting fluid driven by thermal convection in the incompressible case is studied by direct numerical simulations at Rayleigh numbers up to 200 times critical and Prandtl numbers 0.2 and 1. Our results are consistent with a dynamo effect which occurs for magnetic Reynolds numbers above a few tens, in the presence of, as well as in the absence of, rotation around the vertical axis. In all cases, the magnetic field is more intermittent than the velocity field.

1. The dynamo problem

We report here the results of a numerical study of the enhancement of magnetic fields through turbulent motions in a horizontal layer of electrically conducting fluid heated from below. This 'turbulent dynamo' effect is generally invoked to explain the observed fields of planets, stars and galaxies. The stretching of magnetic field lines by velocity gradients may, when the magnetic Reynolds number Re_m is large enough, overcome the Joule dissipation. Re_m is defined as $v_0 l_0/\eta$, where l_0 and v_0 are respectively a typical large scale length and velocity, and η is the magnetic diffusivity. The magnetic Reynolds number measures the characteristic time ratio of the afore-mentioned two physical processes.

The dynamo effect is difficult to observe in the laboratory, where typical magnetic Reynolds numbers are too low. Experiments to measure the ambient magnetic field in the sodium cooling system of the breeder reactor Superphenix are underway. The size of this plant is indeed such that the magnetic Reynolds numbers may be supercritical (Leorat, Pouquet & Frisch 1981). A similar experiment was performed in the Soviet breeder reactor BN 600. A magnetic field was observed which does not seem to be generated by a dynamo effect, but rather by a thermoelectric effect (Kirko *et al.* 1983).

From a theoretical point of view, most works concern the 'kinematical' dynamo case, in which the velocity field $\boldsymbol{v}$, or its small-scale statistics in the tubulent case, is given. The most important theoretical result, in the turbulent context, concerns the 'alpha'-effect (Steenbeck, Krause & Radler 1966), which shows that large-scale magnetic fields are strongly amplified by small-scale velocity fields which possess a large helicity, i.e. a large correlation between velocity and vorticity. In the non-helical case, however, the outcome is less clear, since the two competing effects – that of stretching by velocity gradients and that of enhanced Joule dissipation through nonlinear transfer – have the same characteristic times (Kraichnan & Nagarajan 1967). Lower bounds on the critical magnetic Reynolds number above which a dynamo sets in have nevertheless been obtained in the case of simple flows (see

Moffatt 1978 for references). The self-consistent helical problem, in which the reaction of the magnetic field on the flow through the Lorentz force is taken into account, has been treated analytically by an appropriate modelling of the nonlinear terms (Moffatt 1972; Pouquet, Frisch & Leorat 1976), and more recently by multiple-scale analysis (Montgomery & Hatori 1984; Chen & Montgomery 1986; Matthews, Goldstein & Lantz 1986). In the three-dimensional case, these studies emphasize the importance of magnetic helicity (correlation between magnetic potential and field) in the saturation of the large-scale helical dynamo mechanism. In the non-helical case, it was shown in Leorat *et al.* (1981, hereinafter referred to as paper I) using second-order closure techniques, that in the presence of a driving force for the velocity field a magnetic steady state obtains above a critical magnetic Reynolds number $Re_{\rm mc}$ of the order of 30. It should be noted that in this case the instability is of a local type, the magnetically excited scales being of the same order as those of the turbulent velocity field: one thus speaks of a small-scale dynamo. More recently, Gilbert, Frisch & Pouquet (1988) has shown for an explicit example that a large-scale dynamo can obtain in the non-helical case provided that the small-scale turbulence be non-parity-invariant. The analysis is that of the standard alpha-effect, but one order further in the expansion parameter (small-scale magnetic Reynolds number). The study of its nonlinear saturation is underway, both analytically and numerically.

Another method to study the nonlinear self-consistent problem, more akin to experimentation, consists of three-dimensional direct numerical simulations. However, even on the largest available computers, one is presently restricted to rather modest Reynolds numbers, whereas such limitations on closures are less stringent, because of the exponential discretization used. Numerical experiments were done in the homogeneous turbulent case (Meneguzzi, Frisch & Pouquet 1981, hereinafter referred to as paper II) in the simplest possible geometry, i.e. periodic boundary conditions in all directions, with random forcing as the mechanical energy source. A small-scale dynamo effect in the absence of helicity (Zero helicity spectrum) was observed above a critical magnet Reynolds number of order 40, in agreement with closure calculations.

Random forcing allows close comparison with theoretical works using closures; on the other hand, buoyancy provides a more physical and yet simple forcing to the velocity field. Several numerical experiments of three-dimensional magnetoconvection have been presented (Gilman & Miller 1981; Glatzmaier & Gilman 1982; Glatzmaier 1984). This series of works considers a spherical shell, with the solar dynamo in mind. In the present paper, we do not wish to address the solar dynamo problem in particular, but rather consider questions of a more basic nature, namely what are the ingredients necessary to produce a turbulent dynamo. For this purpose, we use the simplest geometry, in order to maximize the space resolution and minimize the integration time. We first review briefly the numerical method in §2 and describe several of the tests performed on our code in §3. The results in the non-rotating and in the rotating cases are presented in §4 and 5 respectively, and a discussion follows in §6.

2. The numerical method

We consider a flat infinite layer of fluid heated from below. The three-dimensional MHD equations, in the Boussinesq approximation, are in non-dimensional form

$$\frac{\partial \boldsymbol{v}}{\partial t} = \boldsymbol{v}\times\boldsymbol{\omega} + \boldsymbol{j}\times\boldsymbol{b} - \nabla\Pi + Ra\,Pr\,\theta\,\boldsymbol{e}_z + Pr\,\nabla^2\boldsymbol{v} + 2\boldsymbol{\Omega}\times\boldsymbol{v}, \tag{1}$$

$$\frac{\partial \boldsymbol{b}}{\partial t} = \boldsymbol{\nabla} \times (\boldsymbol{v} \times \boldsymbol{b}) + \frac{Pr}{P_{rm}} \boldsymbol{\nabla}^2 \boldsymbol{b}, \tag{2}$$

$$\frac{\partial \theta}{\partial t} = -\boldsymbol{\nabla} \cdot (\boldsymbol{v}\theta) + v_z + \nabla^2 \theta, \tag{3}$$

$$\boldsymbol{\nabla} \cdot \boldsymbol{v} = \boldsymbol{\nabla} \cdot \boldsymbol{b} = 0. \tag{4}$$

We have taken as units of length, temperature and time respectively the height h of the layer, the temperature difference between bottom and top $\Delta T = T_0 - T_1$ and the thermal diffusion time through the layer h^2/χ (χ is the thermal diffusion coefficient). In these equations, $\boldsymbol{v}$ is the velocity field, $\boldsymbol{b}$ the Alfvén speed (proportional to the magnetic induction $\boldsymbol{B}$), θ the temperature fluctuation with respect to the conductive profile $T_0 - z\Delta T$, Π the total pressure $p + \frac{1}{2}v^2$, Ra the Rayleigh number, Pr the Prandtl number and Pr_m the magnetic Prandtl number ν/η, where ν is the kinematic viscosity and η the magnetic diffusivity. Finally, $\boldsymbol{e}_z$ is the unit vector in the vertical direction z, $\boldsymbol{\omega} = \boldsymbol{\nabla} \times \boldsymbol{v}$ is the vorticity and $\boldsymbol{j} = \boldsymbol{\nabla} \times \boldsymbol{b}$ is proportional to the current density. Finally, Ω is the rotation around the vertical axis. The viscous and Joule source terms are omitted in the heat equation since they are small compared with the remaining terms (see Chandrasekhar 1961).

The equations are integrated using a Fourier spectral method (see Gottlieb & Orszag 1977). The computation of derivatives and the time stepping are performed in Fourier space. The nonlinear terms are computed in real space using fast Fourier transforms. The time stepping is done by leapfrog for the nonlinear terms and by an implicit scheme (Cranck–Nicolson) for the coupling terms between the equations of $\boldsymbol{v}$ and $\boldsymbol{b}$. For the dissipative terms, we use the following method (Basdevant *et al.* 1981): making the change of variables (in Fourier space)

$$\boldsymbol{v}' = \boldsymbol{v} \exp(Pr\, k^2 t), \quad \boldsymbol{b}' = \boldsymbol{b} \exp(k^2 t Pr/Pr_m), \quad \theta' = \theta \exp(k^2 t),$$

then discretizing the equations and returning to the original variables, one obtains the scheme

$$\frac{\boldsymbol{v}^{n+1} - \boldsymbol{v}^n \exp(-2Pr\, k^2 \delta t)}{2\delta t} = \boldsymbol{P}(k) \cdot (\boldsymbol{v}^n \times \boldsymbol{\omega}^n + \boldsymbol{j}^n \times \boldsymbol{b}^n - \boldsymbol{\nabla}\Pi^n) \exp(-Pr\, k^2 \delta t) + Pr\, Ra\, \boldsymbol{e}_z \tfrac{1}{2}(\theta^{n-1} \exp(-2Pr\, k^2 \delta t) + \theta^{n+1}), \tag{5}$$

$$\frac{\boldsymbol{b}^{n+1} - \boldsymbol{b}^n \exp(-2Pr\, k^2 \delta t/Pr_m)}{2\delta t} = \mathrm{i}\boldsymbol{k} \times (\boldsymbol{v}^n \times \boldsymbol{b}^n) \exp(-Pr\, k^2 \delta t/Pr_m), \tag{6}$$

$$\frac{\theta^{n+1} - \theta^n \exp(-2k^2 \delta t)}{2\delta t} = \mathrm{i}\boldsymbol{k}(\boldsymbol{v}^n \theta^n) \exp(-k^2 \delta t) + \tfrac{1}{2}[v_z^{n+1} + v_z^{n-1} \exp(-2k^2 \delta t)], \tag{7}$$

with the tensor $\boldsymbol{P}$ defined as $P_{ij} = (\delta_{ij} - k_i k_j)/k^2$.

Aliasing is removed in some of our runs by a method due to Patterson & Orszag (1971), which requires no additional memory but doubles the integration time. The spectral (i.e. dealiased) version of the scheme allows one to reach higher Rayleigh numbers for a given space resolution than with the pseudospectral (i.e. aliased) version. This is, however, at the cost of misrepresenting somewhat the small-scale dissipation. Finally, to prevent the marginal instability of the leapfrog scheme from developing, we mix the last three time-steps sporadically according to

$$\theta^n = \tfrac{1}{4}(\theta^{n-1} + 2\theta^n + \theta^{n+1}),$$

which preserves the second-order accuracy of the scheme. We use periodic boundary

conditions in the horizontal directions, and free-slip stress-free conditions in the vertical direction, i.e. we have at the top and bottom of the layer

$$v_z = \partial_z v_x = \partial_z v_y = 0.$$

The same boundary conditions apply to the magnetic field if the external medium is a perfect electrical conductor (see Chandrasekhar 1961). For θ, the conditions are $\theta = 0$ at $z = 0$ or 1. This allows us to expand the fields in sine or cosine series with respect to the vertical coordinate z. The spatial resolution is typically $48 \times 48 \times 24$ on a 1 Megaword CRAY-1 computer, and $64 \times 64 \times 32$ on a 2 Megaword CRAY-XMP. The corresponding time-steps take 5 and 10 s respectively (40 % of which is time waiting for I/O). As a last point, let us stress that we present only results of 'direct' simulations, i.e. no parametrization of the small scales (through a turbulent viscosity model, for example) is used in our runs.

3. Tests of the code

As a first test, we have computed the critical Rayleigh number for the onset of convection. Our results are consistent with the known value of $Ra_c = 657.5$ in the case of free-slip boundaries. For a Prandtl number of 0.2, just above the threshold, convection is in the form of two-dimensional rolls. We have computed the critical Rayleigh number for the transition to three-dimensional convection through the oscillatory instability and found excellent agreement with the value given in Clever & Busse (1974). The comparison is presented in Meneguzzi *et al.* (1987), a paper devoted to the transition to turbulent convection at low Prandtl numbers.

A second test consisted in calculating the Nusselt number as a function of the Rayleigh number for Ra/Ra_c ranging from 1 to 150. The Nusselt number is defined as the ratio of the mean vertical heat flux to the flux that would occur with pure conduction. It is given, in non-dimensional units, by

$$Nu = \overline{v_z \theta - \partial_z \theta}, \tag{8}$$

where the bar means horizontal average. Since our free-slip boundary conditions do not allow for a straight comparison with laboratory experiments, we confront our results with those of previous computations. Figure 1 shows our calculated values together with the curve obtained by Moore & Weiss (1973) for two-dimensional numerical simulations, at $Pr = 1$. The agreement with the Moore & Weiss result is excellent up to a Rayleigh number 80 times critical. The power law apparent in figure 1 has an exponent close to (but not exactly) $\frac{1}{3}$. Such an exponent can readily be obtained by assuming that convection acts to produce a nearly isothermal layer of fluid, and that heat diffusion only occurs in the thermal boundary layers (Spiegel 1971). This argument does not depend on the space dimensionality, and is therefore consistent with the good agreement we find. Note that for $Pr = 1$, the results of direct simulations by Curry *et al.* (1984) indicate that the flow is three-dimensional for $Ra > 40\, Ra_c$. The discrepancy at Ra/Ra_c larger than 80 may be a real effect, due to a smaller integral scale of three-dimensional turbulent convection and thus less efficient turbulent heat transport. However, with such runs we are reaching the upper limits of the Rayleigh numbers that can be simulated without serious truncation error. This point remains to be explored, but is not central to our paper.

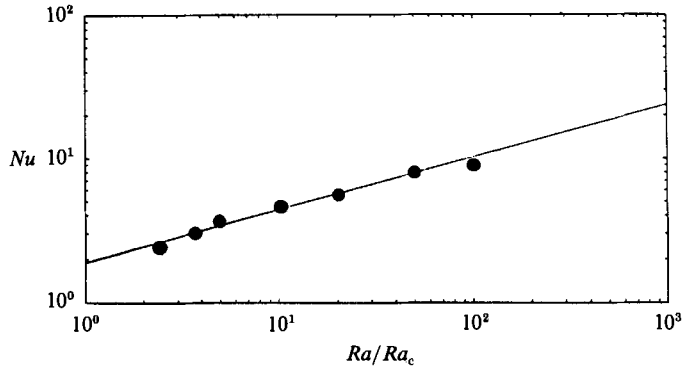

FIGURE 1. Nusselt number Nu as a function of the Rayleigh number Ra/Ra_c. The solid line is from the two-dimensional results of Moore & Weiss (1973) and the dots show our results. Note that the three-dimensionality effects are seen only at large Rayleigh number.

4. Convective dynamo without rotation

We want to study the bifurcation from a statistically stationary turbulent regime without a magnetic field to a regime with a finite-amplitude $\boldsymbol{b}$-field. An initial amplification of the magnetic field always occurs, but this field will eventually die out when the magnetic Reynolds number is too low.

Each of our runs is characterized by four parameters: the Rayleigh number Ra, which is essentially the magnitude of the buoyancy force, the Prandtl number Pr and magnetic Prandtl number Pr_m, and the rotation rate $\boldsymbol{\Omega}$, which is zero for the runs considered in this Section. For given Ra and Pr parameters, a Reynolds number Re results and the magnetic Reynolds number Re_m obtains from the magnetic Prandtl number ($Re_m = Pr_m Re$). Theoretical considerations (Batchelor 1950; Schlüter & Biermann 1950) as well as previous numerical studies (Papers I and II, and Gilman & Miller 1981) suggest that Re_m is the one parameter governing the existence (or lack thereof) of the dynamo effect, provided the (kinetic) Reynolds number is high enough for the small-scale flow to be turbulent. The characteristics of all the runs presented in this paper are summarized in table 1. In this table, N is the number of Fourier modes in each horizontal space direction (the number of modes in the z-direction is $\frac{1}{2}N$), E_m and E_v are the volume-averaged magnetic and kinetic energy, Ro is the Rossby number, defined as $v_0/\Omega h$. Re_λ is the Reynolds number based on the Taylor microscale, which, in the present Reynolds-number range, does not differ much from the Reynolds number based on the integral scale l_0 (see table 1). Let us recall the definitions of l_0 and λ:

$$l_0 = \int \mathrm{d}k E_v(k)/k / \int \mathrm{d}k E_v(k), \tag{9}$$

$$\lambda^{-2} = \int \mathrm{d}k E_v(k)\, k^2 / \int \mathrm{d}k E_v(k). \tag{10}$$

In order to maximize the Reynolds number, we compute at the highest Rayleigh number allowed by our spatial resolution, which is of the order of 100 to 200 times the critical Rayleigh number Ra_c for the onset of convection. We let the flow evolve without a magnetic field until a statistically stationary regime sets in. At slightly supercritical Rayleigh numbers (see below, figure 6), the size of the energy-containing cells is of the order of the depth of the layer h, whereas at higher Rayleigh numbers this is no longer the case. For the N3 run, the typical size of the large eddies varies in time between h and $\frac{1}{3}h$. The temperature profile is shown in figure 2 and its

RUN	N	Ra/Ra_c	Pr	Pr_m	Ro	Re	Re_m	Dynamo	E_m/E_v	Re_λ
N1	48	100	1	3	∞	16	50	no	—	12
N2	48	100	1	5	∞	20	100	?	—	13
N3	64	100	1	7	∞	24	170	Yes	3×10^{-4}	15
N4	48	100	1	10	∞	22	220	yes	1.5×10^{-2}	17
N5	48	100	1	7	∞	32	220	yes	3×10^{-4}	20
N6	64	150	1	5	∞	28	140	yes	2×10^{-2}	16
N7	40	150	0.2	3	∞	20	60	yes	2×10^{-2}	10
N8	64	200	0.2	2	∞	100	200	yes	5×10^{-3}	40
N9	64	200	0.2	1	∞	90	90	?	10^{-3}	37
R1	48	150	1	3	0.5	15	45	no	—	10
R2	48	150	1	5	0.5	15	75	yes	5×10.4	10
R3	48	150	1	10	0.5	15	150	yes	10^{-2}	9
R4	40	150	0.2	1	1	45	45	no	—	27
R5	40	150	0.2	2	1	45	90	yes	7×10^{-3}	27
R6	40	150	0.2	3	1	40	115	yes	7×10^{-2}	27

TABLE 1. Identification of the runs reported in this paper. The Rayleigh number Ra is measured in units of the critical Rayleigh number for the onset of convection Ra_c, Pr is the Prandtl number, Pr_m the magnetic Prandtl number, Ro is the Rossby number, Re the Reynolds number based on the integral scale, Re_m the magnetic Reynolds number and Re_λ the Reynolds number based on the Taylor microscale. Note that in the presence of rotation, the dynamo appears more efficient since it can occur at lower Pr_m. The number of Fourier modes is N in the $x-$ and y-directions and $\frac{1}{2}$N in the z-direction.

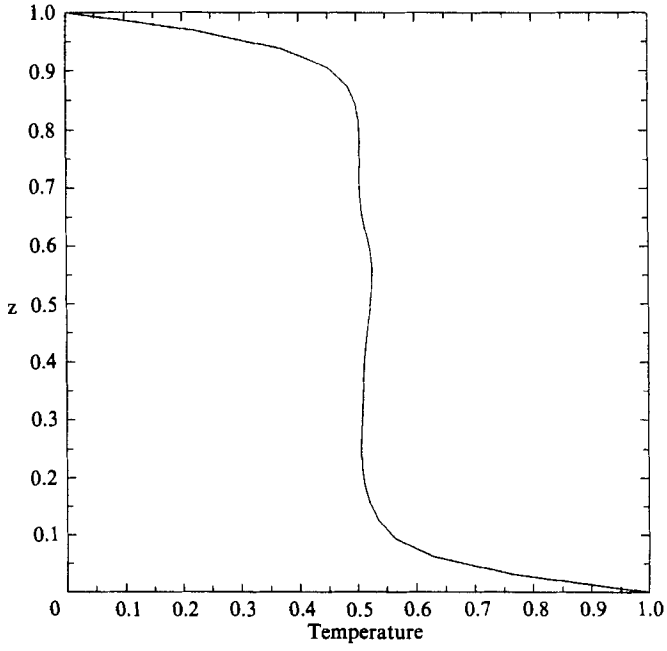

FIGURE 2. Temperature profile across the convection layer before the magnetic seed is introduced. $Ra/Ra_c = 110$, $Pr = 1$. Note the quasi-isothermal region inside the box, surrounded by two thermal boundary laters.

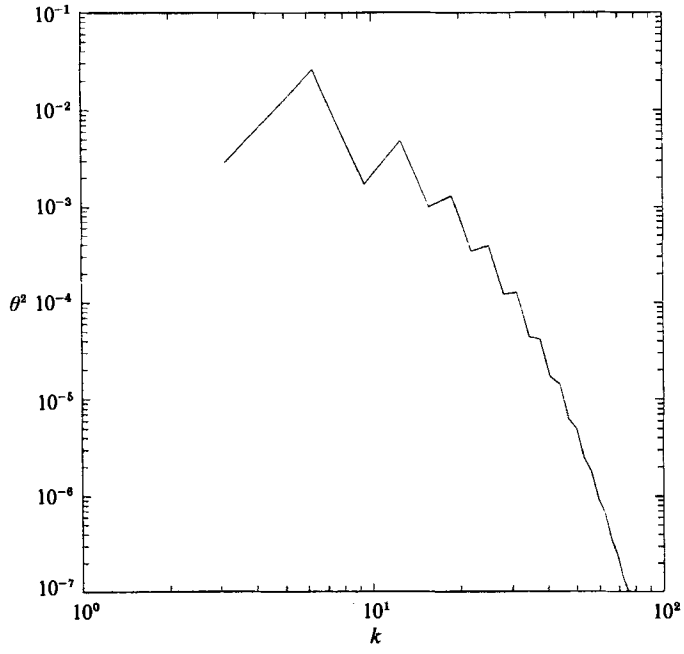

FIGURE 3. Spectrum of the temperature fluctuations (with respect to the conductive profile) for the same conditions as in figure 2. Note the broad range of excited modes.

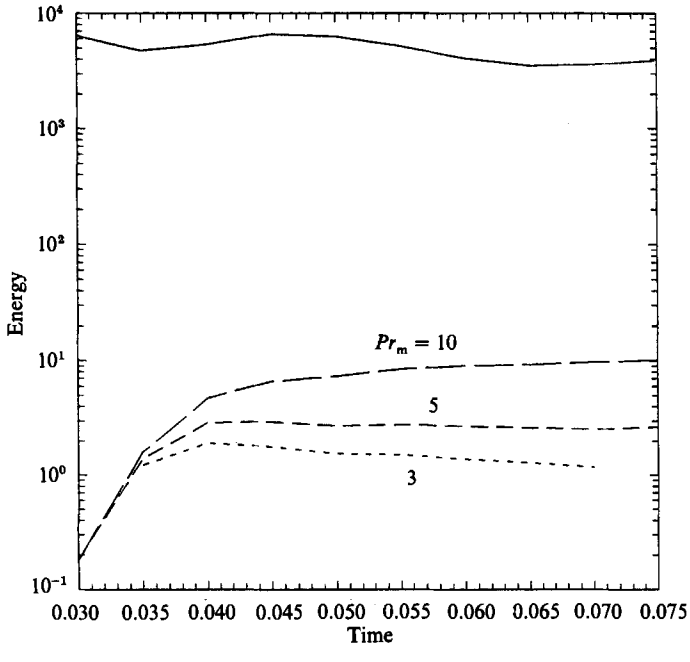

FIGURE 4. Temporal variation of kinetic (solid line) and magnetic (dashed lines) energy for various magnetic Prandtl numbers (indicated on the curves). $Ra/Ra_c = 100$, $Pr = 1$, no rotation

(*a*)(i)

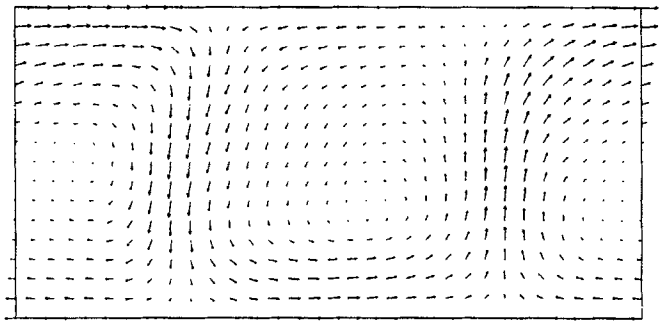

(*a*)(ii)

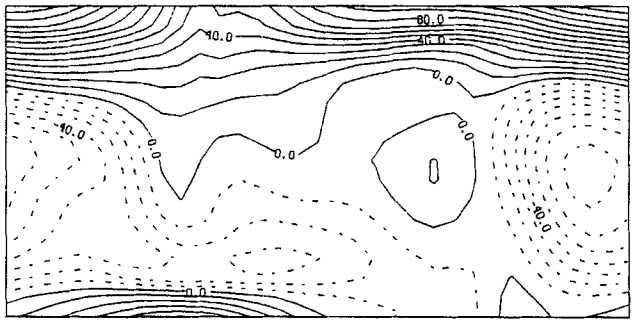

(*b*)(i)

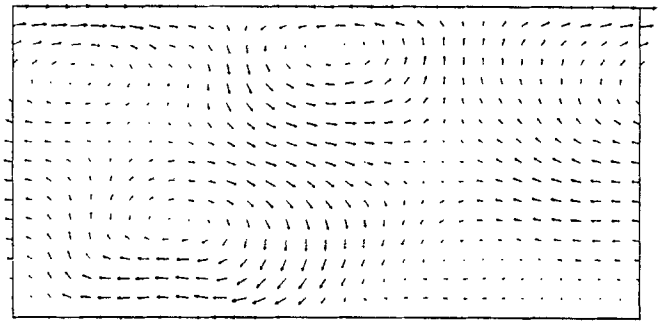

(*b*)(ii)

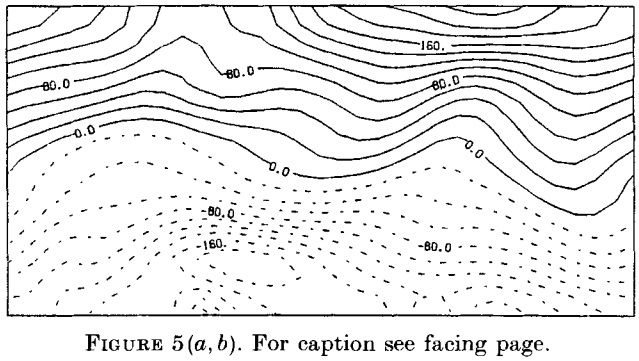

FIGURE 5(*a*, *b*). For caption see facing page.

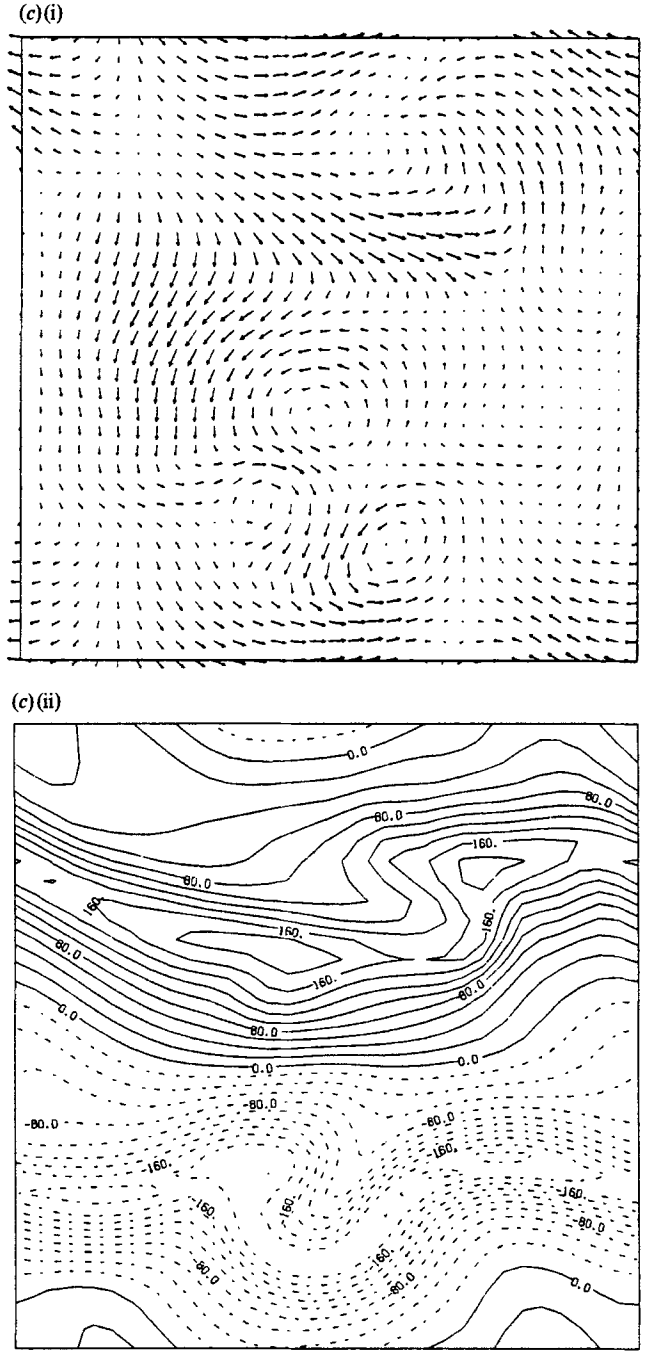

FIGURE 5. (*a*) (i) Projection of the velocity field on plane $x = 0$; (*a*) (ii) contour plot of the x-component; (*b*) as (*a*) but for plane $y = 0$; (*c*) as (*a*) but for $z = 0.5$. Run N6.

(a)(i)

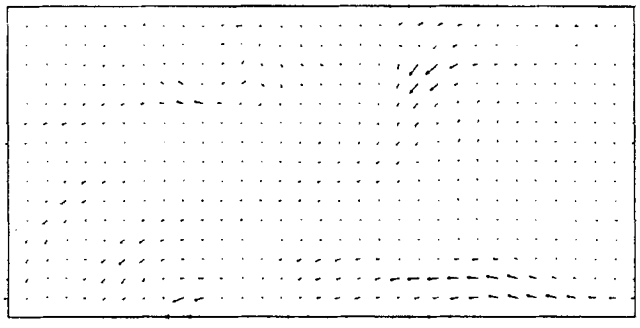

(a)(ii)

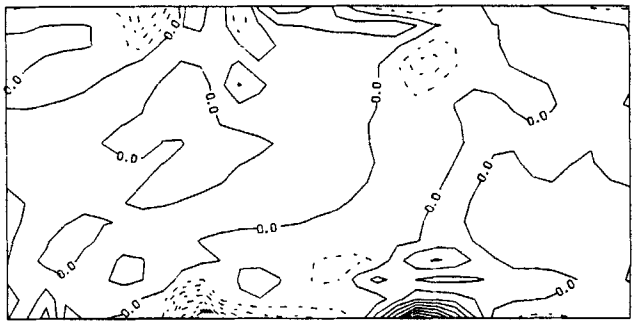

(b)(i)

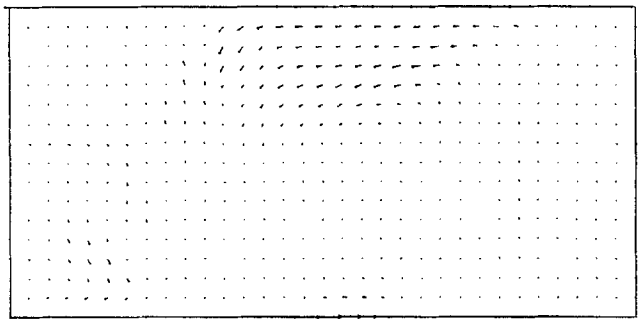

(b)(ii)

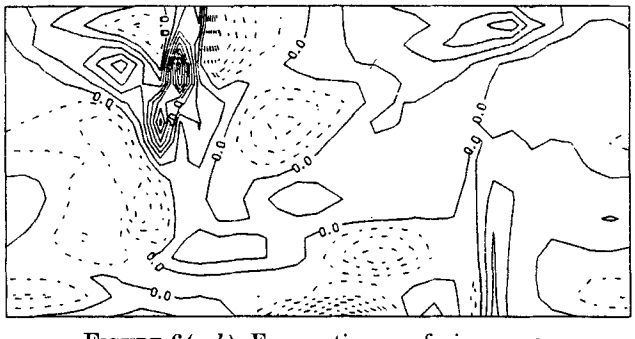

FIGURE 6(a, b). For caption see facing page.

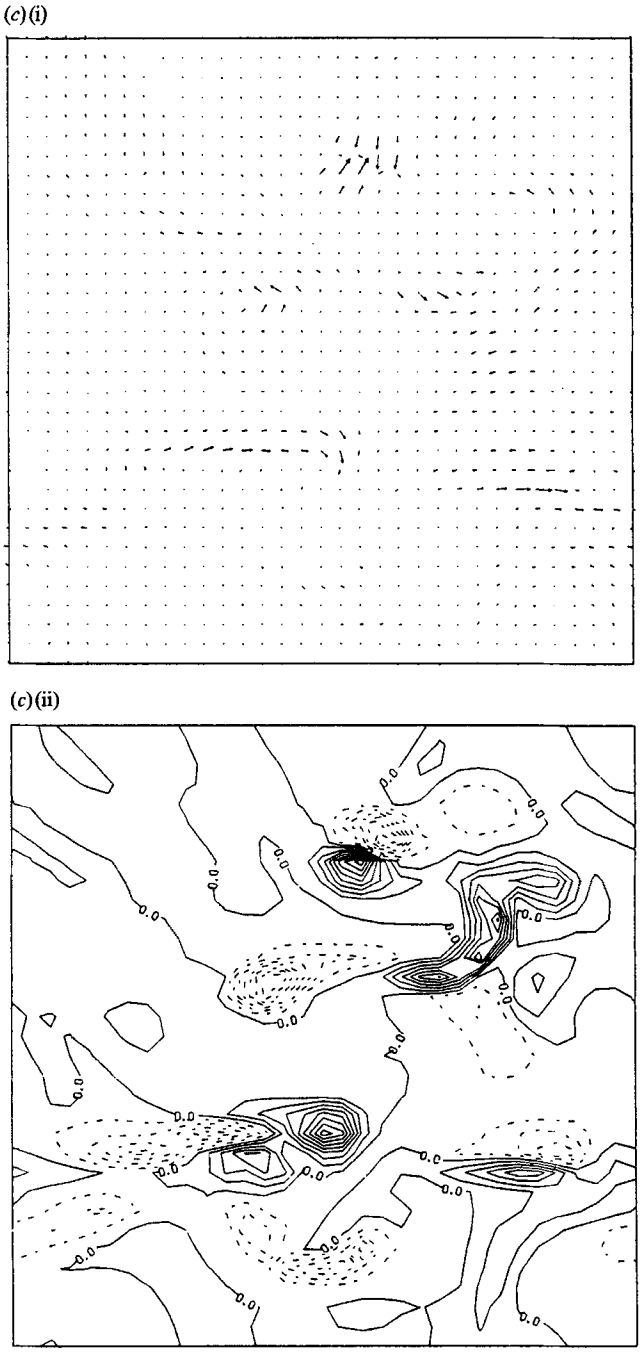

FIGURE 6. Same as figure 5 for the magnetic field.

spectrum in figure 3. As expected, the flow displays a roughly isothermal central part, surrounded by the upper and lower thermal boundary layers. Note also that convection provides a forcing of the velocity field in a wide range of wavenumbers.

After a statistically stationary state has developed, we introduce a seed magnetic field of low intensity ($E_m/E_v \approx 5 \times 10^{-5}$) and confined to the large scales of the flow,

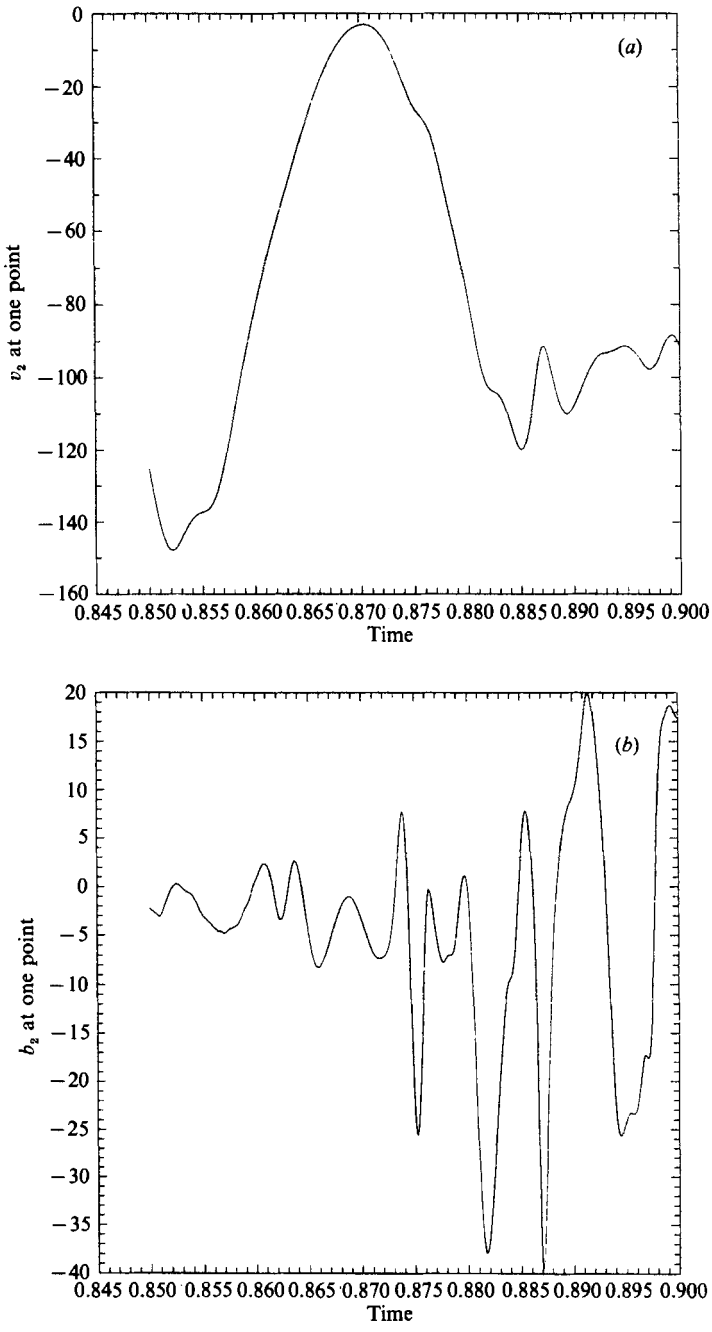

FIGURE 7. Temporal variation of the y-component of (a) the velocity and (b) the magnetic field for run N6 at a given point in space. Note the faster timescale of the magnetic field variation.

and look at its eventual fate for times long compared with the large-scale eddy turnover time, which is of the order 0.01 in our calculations. We show in figure 4 the evolution of the kinetic (upper curve) and magnetic (lower curves) energies as a function of time for various magnetic Prandtl numbers Pr_m. We see that, in the units chosen here, the r.m.s. velocity is approximately equal to 100, while the r.m.s. Alfvén

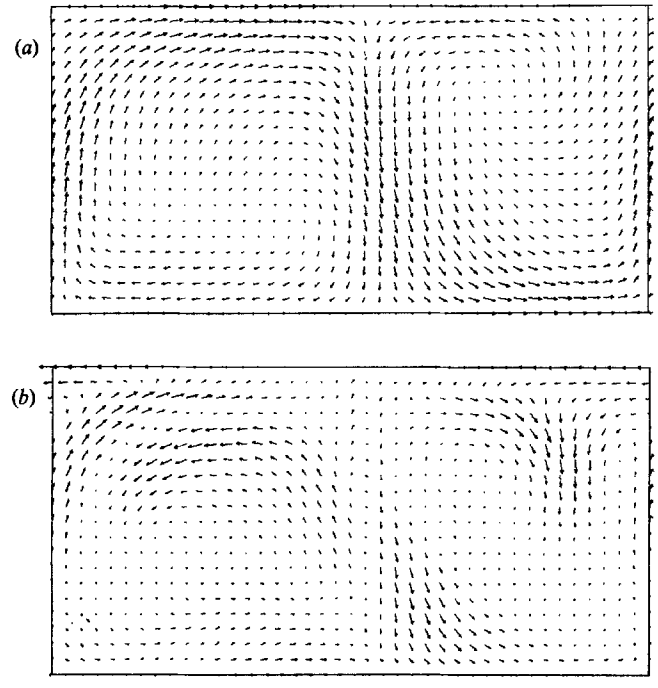

FIGURE 8. Projection of (*a*) the velocity and the (*b*) magnetic field onto the $x = 0$ plane; $Ra/Ra_c = 80$, $Pr = Pr_m = 1$.

speed stabilizes at around 2 in the least favourable case ($Pr_m = 5$). This corresponds to a value of Re_{mc} of around 100, slightly larger but not inconsistent with the results of random forcing studies (paper II) and closure calculations (paper I). Note that in all three studies, the Reynolds number is computed using the integral scale l_0 (see (9)), and that for comparison with laboratory studies, such Reynolds numbers should be upgraded by a factor 2π. We show in figures 5 and 6 respectively the velocity and magnetic fields projected onto three orthogonal planes for run N6. The typical scales of $\boldsymbol{b}$ and $\boldsymbol{v}$ are the same but, as we found in the random forcing case (paper II), $\boldsymbol{b}$ is more intermittent than $\boldsymbol{v}$. This can also be deduced from the fact that although most of the energy of the flow is in kinetic form, the maximum values of $\boldsymbol{b}$ and $\boldsymbol{v}$ are roughly equal. The origin of such an intermittent behaviour is not clear. It could be because we are close to the transition from a non-magnetic to a magnetic state; indeed, owing to the lack of spatial resolution, only slightly supercritical dynamos have been obtained up to now by direct numerical simulations. If this were the case, the intermittency of $\boldsymbol{b}$ observed here should disappear at higher Re_m. On the other hand, this intermittency could be of a dynamical nature. For example, $\boldsymbol{b}$ may grow preferentially where strong velocity gradients are present, or in regions of high vorticity. In fact, there appears to be some correlation between the magnetic field $\boldsymbol{b}$ and the vorticity $\boldsymbol{\omega}$. This may be attributed to the fact that both variables follow similar equations when close to the kinematical case ($E_m \ll E_v$) (Batchelor 1950). We show in figure 7 the temporal evolution of the velocity (7*a*) and of the magnetic field (7*b*) at a given point in space, away from the boundaries. The magnetic field exhibits a more rapid, probably chaotic (Meneguzzi *et al.* 1987), behaviour than the velocity. Note that the characteristic scale of $\boldsymbol{b}$ is smaller than that of $\boldsymbol{v}$, the Alfvén wave

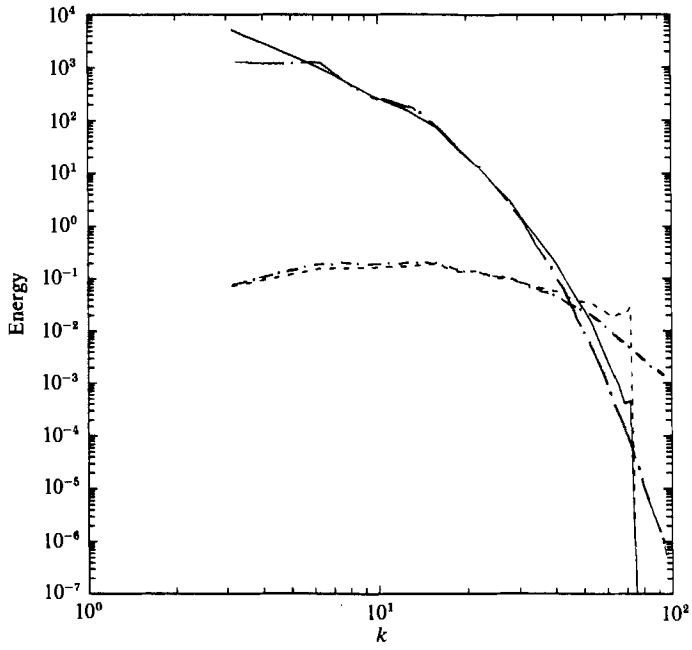

FIGURE 9. Kinetic (solid line) and magnetic (dashed line) energy spectrum at $t = 0.14$. The results of two calculations at different resolution are shown: run N5 ($N = 48$) and run N3 ($N = 64$, curves with inserted dots).

mechanism (Pouquet *et al.* 1976) being faster and thus more efficient at small scales. It may also be linked to the spatial intermittency of $\boldsymbol{b}$.

At these Rayleigh numbers and in the dynamo regime, no conspicuous correlation seems to exist between $\boldsymbol{b}$ and $\boldsymbol{v}$ itself. This is not the case at moderate Rayleigh numbers, as can be seen in figure 8, where the $\boldsymbol{v}$- and $\boldsymbol{b}$-field projections on a vertical plane are shown for $Ra = 50Ra_c$, $Pr = 1$ and $Pr_m = 2$.

Information on the flow can also be obtained using statistical quantities, such as shell-averaged Fourier spectra. In our runs at Prandtl numbers of order unity, no serious truncation is seen for the kinetic energy spectrum, for which the small scales are well resolved. Such is not the case for the magnetic field when the magnetic Reynolds number is high. The question then arises as to whether underestimating the Joule dissipation – owing to the lack of small-scale resolution in $\boldsymbol{b}$ – could affect our results. In order to check this we have performed two runs with the same values of the parameters but with resolutions $N = 48$ (run N5) and $N = 64$ (run N3). Figure 9 shows the energy spectra obtained in these runs. The discrepancy in the large scales is due to a combination of large fluctuations (there is a small number of points in the first few shells over which spectra are averaged), and to the fact that the random initial conditions centred in the large scales are not identical in the two runs. On the other hand, truncation shows up in the small scales, but the two spectra are nevertheless comparable. The dynamo effect present in the $N = 48$ run is also present in the $N = 64$ one, with roughly the same magnetic energy. This suggests that the flow is well resolved and that qualitatively, our results on the existence of a dynamo effect produced by turbulent convection are correct.

The slight excess of magnetic energy over its kinetic counterpart at small scales shown in figure 9 could be due to the fact that the magnetic Prandtl number Pr_m is

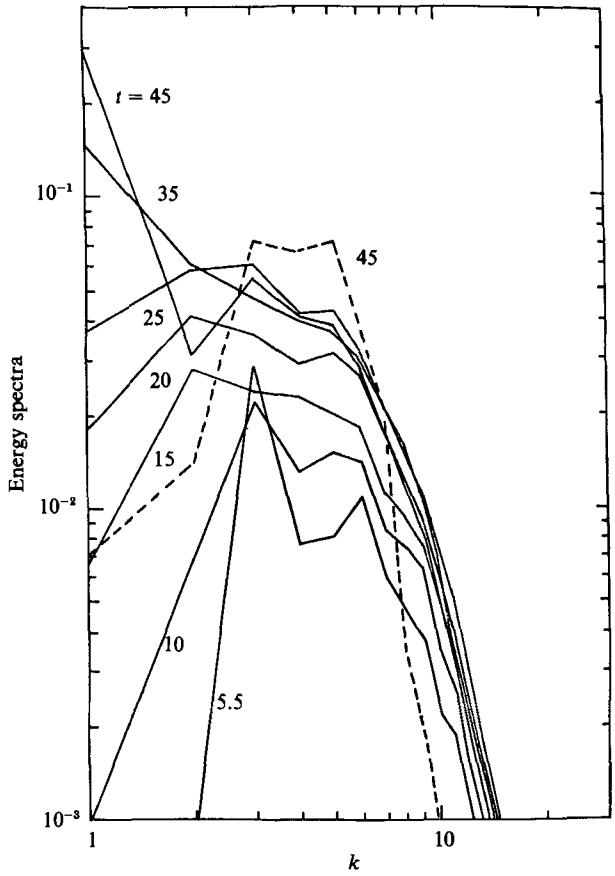

FIGURE 10. Growth of large-scale magnetic energy for a run with random forcing due to inverse cascade of magnetic helicity. Continuous lines: magnetic energy spectra at different times, given on the curves; dashed line: kinetic energy spectrum at $t = 45$. Here, the unit time is the large-scale eddy-turnover time.

above unity. However, we should note that in all the runs we have performed, both in the convective and in the random forcing case, in three as well as in two dimensions, and also in closure calculations, this is most often the case. It is also found in satellite observations of the solar wind (Smith, Matthaeus & Goldstein 1983).

5. The role of helicity

Helicity is known to play an important role, although not a necessary one, in the dynamo problem (see for example Moffatt 1978; Parker 1979; Zeldovich, Ruzmaikin & Sokolov (1983); and also papers I and II). It is defined as $\langle \boldsymbol{v}\cdot\boldsymbol{\omega}\rangle$, where $\langle\,\rangle$ means space average and $\boldsymbol{\omega} = \text{curl}\ \boldsymbol{v}$. We use here the relative helicity $H = \langle \boldsymbol{v}\cdot\boldsymbol{\omega}\rangle/\langle v^2\omega^2\rangle^{\frac{1}{2}}$. A velocity field is said to have maximal helicity when $H = \pm 1$. Similarly, magnetic helicity $H_{\rm m}$ is defined as $\langle \boldsymbol{a}\cdot\boldsymbol{b}\rangle$, where $\boldsymbol{a}$ is the magnetic potential. It has been conjectured on a statistical basis (Frisch *et al.* 1975) and found in second-order closure calculations (Pouquet *et al.* 1976) that $H_{\rm m}$ undergoes an inverse cascade towards large scales. This induces a growth of the large-scale magnetic field itself.

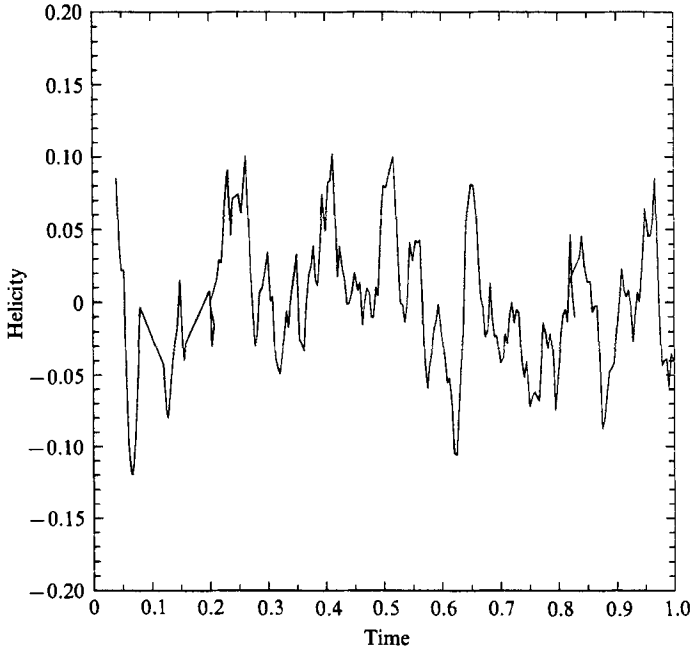

FIGURE 11. Temporal variation of the relative kinetic helicity for a run without rotation (run N6) and $Ra/Ra_c = 150$, $Pr = 1$, $Pr_m = 5$.

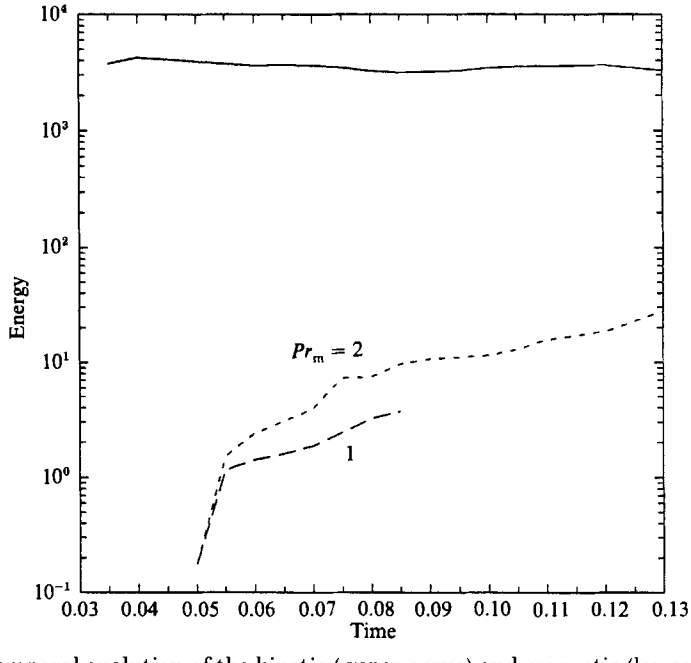

FIGURE 12. Temporal evolution of the kinetic (upper curve) and magnetic (lower curves) energy for various magnetic Prandtl numbers (as labelled on the curves). $Ra/Ra_c = 200$, $Pr = 0.2$ and no rotation.

This effect is observed in MHD numerical simulations (paper II) (see also Zeldovich *et al.* 1983, p. 191). In figure 10, we show as a function of time the magnetic energy spectrum obtained in one of the 32^3 runs presented in paper II (solid lines), with the kinetic energy spectrum (dashed line) having reached a steady state. In this simulation, the flow was homogeneous, and the mechanical energy source was represented by a narrow-band (in Fourier space) random forcing term in the velocity equation, with a high helicity. In the unforced case, it is likely, that only a positive energy transfer at large scales can obtain (Pouquet & Patterson 1978). Such inverse transfer in Fourier space corresponds to the formation of large-scale force-free structures and is an example of self-organisation in MHD flows.

Contrary to the homogeneous case with random forcing, we cannot in the case of convection impose a given helicity to the $\boldsymbol{v}$-field. Moreover, we cannot impose a narrow-band forcing at a given wavenumber. The forcing due to the temperature gradient covers a wide range of scales (at Prandtl numbers of order 1). An inverse magnetic helicity cascade is therefore difficult to observe. Figure 11 displays the relative kinetic helicity versus time for the run N6. H seems to fluctuate around 0, with $|H|$-values not exceeding the 10% level, although locally the helicity density $\boldsymbol{v}\cdot\boldsymbol{\omega}$ can be higher. These fluctuations occur with a characteristic time of a few eddy turnover times. It has been noted (Kraichnan 1976) that even when the relative helicity is low, spatial fluctuations of helicity density may play an important dynamical role in the dynamo mechanism by leading to a negative turbulent magnetic diffusivity. This may be the basis of the dynamo we observe here. On the other hand, in a recent study (Gilbert *et al.* 1988), it was found that the large-scale magnetic field can become unstable in a non-helical flow (Zero helicity spectrum) provided the small-scale turbulence be non-parity-invariant. Is it possible that local fluctuations of non-parity invariance in a globally parity-invariant flow also produce a negative magnetic diffusivity? No calculation analogous to the one by Kraichnan (1976) has been done yet. Note that in both cases, the theoretical calculations are done for large-scale separation L/l, where L is the scale of the mean magnetic field and l the turbulence scale. It is therefore difficult to state at this point whether one of the above mechanisms is responsible for the dynamos we observe.

Similar calculations were done at $Pr = 0.2$ (runs N7 and N9) to check whether a higher level of turbulence in the small scales would result in a more powerful dynamo. Figure 12 shows the evolution of the magnetic and kinetic energies versus time in this case. We obtain a dynamo effect for lower Pr_{m} than before. However, in terms of magnetic Reynolds number, the results are essentially the same. The value of Re_{mc} is around 100 as in the $Pr = 1$ case. This is consistent with Re_{m} being the relevant parameter of the bifurcation from a pure-fluid state to an MHD state.

6. Convective dynamo in the presence of rotation

The periodic boundary conditions in the x- and y-directions do not allow us to study the dynamo that would be produced by a combination of convection and differential rotation, which is believed to be at the origin of the terrestrial and solar dynamos. We can, however, study the effect of a solid-body rotation $\boldsymbol{\Omega}$ around the vertical axis, which calls for adding a Coriolis force term in the momentum equation. This term is homogeneous and consistent with periodicity in x and y. We chose $\boldsymbol{\Omega}$ so that the Coriolis term has the same order of magnitude as the nonlinear term, i.e. the Rossby number Ro is close to 1. Special flows of this type have been studied by Soward (1974).

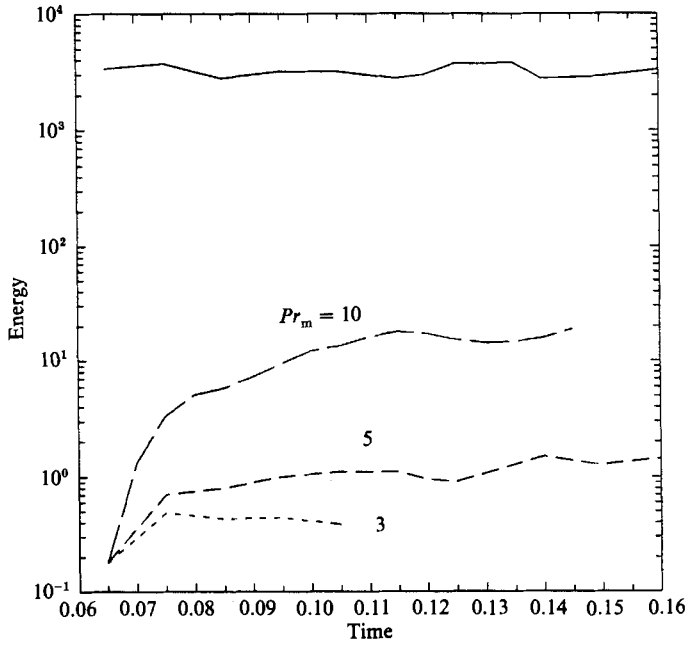

FIGURE 13. Temporal evolution of the kinetic (upper curve) and magnetic (lower curves) energy for various magnetic Prandtl numbers (labelled on the curves) for runs with rotation: $Ra/Ra_c = 100$, $Pr = 1$, $Ro = 0.5$.

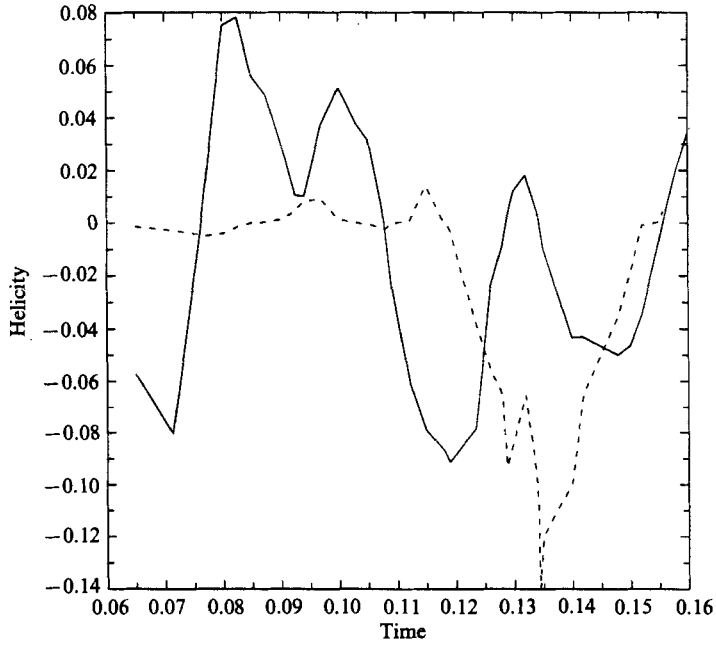

FIGURE 14. Temporal variation of the relative kinetic helicity for a flow with rotation (solid line, $Ro = 0.5$) and without (dotted line); $Ra/Ra_c = 100$, $Pr = 1$, $Pr_m = 5$. Note the similarity both in amplitude and in timescale.

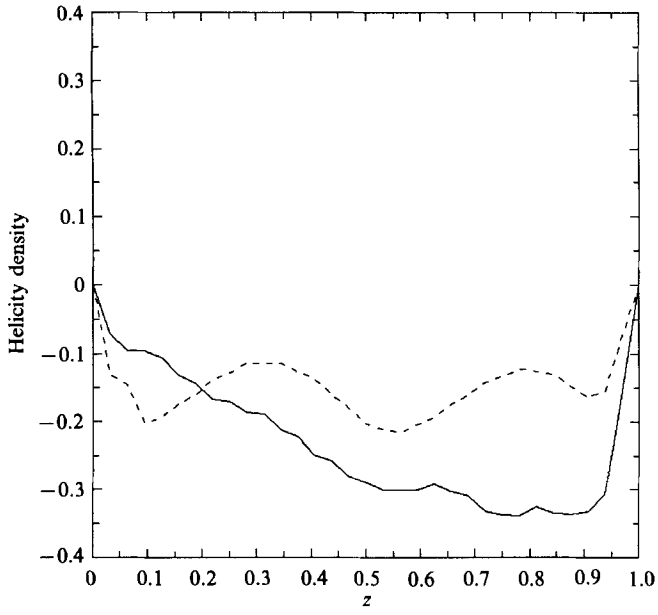

FIGURE 15. Horizontally averaged helicity density as a function of z for runs R6 (solid line) and N6 (dashed line).

Figure 13 shows, as in previous cases, the energies E_m and E_v versus time for different values of Pr_m at $Pr = 1$ and $Ra = 100Ra_c$ (runs R1 to R3). A dynamo effect seems to exist for a value of P_m lower than before. The critical magnetic Reynolds number may therefore be slightly lower than in the non-rotating case. Visualizations of the flow do not show any conspicuous difference to the non-rotating case. Furthermore, as shown in figure 14, the helicity as a function of time seems to behave essentially in the same way as before. We have also repeated the calculations at $Pr = 0.2$ including rotation (runs R4 to R6). Again, the dynamo effect appears at a lower Re_m. One can see from table 1 that in the rotating case Re_m is in the range 45–75, as compared to 100 in the non-rotating case. Note also the higher ratio E_m/E_v that obtains for finite Rossby number, close to 10%. Again, a plot of relative helicity versus time does not show any difference to the case without rotation. Helicity density, however, differs in the rotating and non-rotating case. Figure 15, which shows the horizontally averaged helicity density as a function of z for runs R6 and N6, suggests that, in absolute value, this quantity increases with z in the rotating case R6 (solid line) while it fluctuates around a constant value in the N6 case (dashed line).

7. Discussion

In order to check that the Lorentz force is indeed responsible for the saturation of the magnetic field growth, we have suppressed it in one of our runs (run N10) a little before the end of the linear growth phase. The result is shown in figure 16. One can see that this has no effect during the linear phase, but that the saturation does not occur when the Lorentz force is absent. In the strongly helical case, a description of the saturation mechanism was proposed (Pouquet *et al.* 1976), involving the formation of large-scale force-free fields. But in the non-helical case, the mechanism

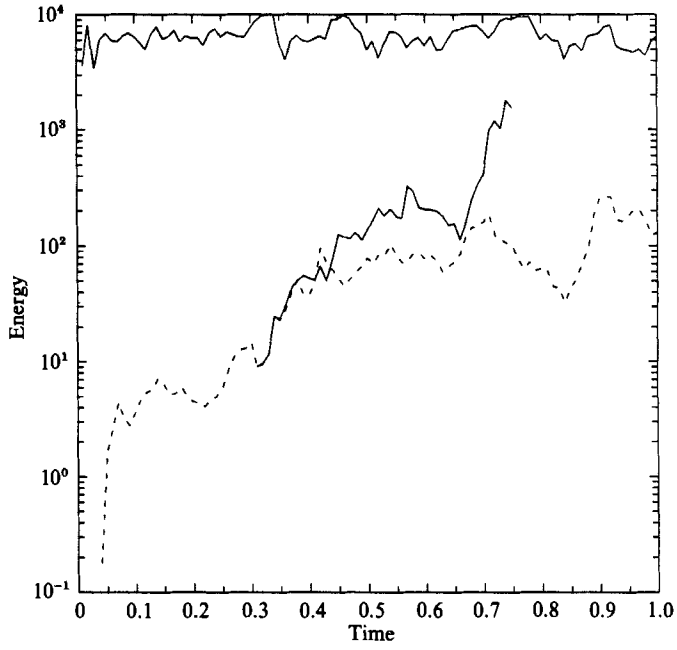

FIGURE 16. Long-time evolution (up to one viscous time) of the total kinetic (upper curve) and magnetic (lower curve, dotted line) energies for run N10. Note the two phases in the growth of the magnetic energy. The lower solid curve shows the result of the removal of the Lorentz force term in the equations.

is less clear. It may be linked to the formation of large-scale coherent structures, which occur through turbulent transfer and nonlinear interactions, and are self-defeating in the sense that they produce force-free fields with maximal kinetic and/or magnetic helicity. It should be recalled here that a force-free state is that predicted by selective decay mechanisms (Matthaeus & Montgomery 1980) in which the energy is minimized while keeping constant the proper physical variables that may be quasi-conserved (magnetic potential in two dimensions, magnetic helicity in three dimensions, and cross-correlation in both dimensions). There have been several recent studies of the behaviour of the helicity in a non-conducting fluid. For example, careful analysis of a three-dimensional channel flow or periodic flow (Shtilman *et al.* 1985) show that force-free helical flows are found mostly in regions of low dissipation and or large scales. In MHD, another possibility to weaken nonlinear interactions through turbulent mode coupling is due to the growth of velocity–magnetic field correlations (Dobrowolny, Mangeney & Veltri 1980; Grappin *et al.* 1981; Matthaeus, Goldstein & Montgomery 1983; Grappin 1986; Pouquet, Meneguzzi & Frisch 1986). In two dimensions, the parameter space has been scanned, in order to determine what are the various regimes that arise (Matthaeus & Montgomery 1984; Ting, Matthaeus & Montgomery 1986). This work remains to be done in three dimensions.

The computational cost of the runs reported here, on a 2 Megawords Cray-XMP, is rather prohibitive. At a resolution of 64^3, it takes 20 hours of CPU time, and twice as much I/O time, to reach $t = 1$ (in units of viscous diffusion times at large scales). Thus we have explored the parameter space letting saturation plateaux establish for moderate times. We have also performed one run at high resolution (N10) up to $t = 1$. For the magnetic Prandtl number simulated here, and considering the fact that

the characteristic scale of the magnetic field that is growing is two to three times smaller than that of the velocity field, this corresponds to roughly one half-Joule dissipation time at those scales. We show in figure 16 the temporal variation of the kinetic and magnetic energy for that run. The magnetic energy, after a first rapid initial growth, saturates until $t = 0.3$; it then undergoes a second slower growing phase (roughly up to $t = 0.5$) and saturates again at a higher value, with small temporal fluctuations. We have looked in detail at the evolution of individual angle-averaged Fourier modes from $k = k_{\min}$ to $k = 7k_{\min}$, and found no prevailing mode in either of the growth phases. This is not surprising since the convective forcing spectrum is broad-band. Finally, let us point out that with a random forcing (paper II), we simulated the flow for two Joule diffusion times of the large scales and observed a continual saturation plateau of the magnetic energy up to the last moment.

In conclusion, our direct three-dimensional numerical simulations show that Boussinesq convection can produce a turbulent dynamo without the help of differential rotation. This may be of particular interest in the solar case, since recent observational data dealing with high-resolution temporal spectra indicate that differential rotation with depth is smaller than previously thought. It is not clear whether the effect we observe can be explained by a negative turbulent diffusivity produced by helicity fluctuations (Kraichnan 1976) or non-parity-invariance fluctuations (Gilbert *et al.* 1988). With present day computers such as the Cray-1 on which we have performed most of our calculations, the lack of resolution is severely felt because of the relatively small available memory. On the next generation of machines, three-dimensional simulations will be the rule rather than the exception. Many questions that have remained unanswered will progressively become accessible. The most urgent, in our opinion, may be to run for several Joule diffusion times a high-resolution non-helical dynamo, either with random forcing or in the convective case. This is now in progress on the Cray-2 of the CCVR. Other problems concern the spatial structure of the magnetic field: does it organize itself in elongated filaments, as in the case of the kinematic dynamo with an ABC flow (Galloway & Frisch 1986)? Does the intermittency of the magnetic field persist well above the critical magnetic Reynolds number? Also of interest is the possible correlation between the growing magnetic field and the vorticity for example, or with other velocity-related variables such as helicity or rate of strain. Such problems require access to powerful and well-resolved visualization equipment with fast three-dimensional software and represent one of the present stumbling blocks of numerical experimentation. Finally, a clear separation between the small-scale turbulence and the large-scale growing field may now be also attainable. This will allow for observing a genuine alpha-effect, and its variants (negative magnetic diffusivity, non-helical non-parity-invariant instabilities, etc...), and should lead to a better theoretical understanding of the long-standing dynamo problem.

We are grateful to D. Galloway and J. Leorat for fruitful discussions. The numerical computations reported here were performed either on the Cray-1S of the Centre de Calcul Vectoriel pour la Recherche, Ecole Polytechnique, Palaiseau or on the Cray-XMP of CISI (Saclay). We are grateful to both. We also want to thank C. Temperton for letting us use his fast Fourier transform code. Finally, the graphics displayed in this paper were done using the software of the National Centre for Atmospheric Research, which is also thanked.

REFERENCES

Basdevant, C., Legras, B., Sadourny, R. & Beland, B. 1981 *J. Atmos. Sci.* **38**, 2305.

Batchelor, G. K. 1950 *Proc. R. Soc. Lond.* A **201**, 405.

Chandrasekhar, S. 1961 *Hydrodynamic and Hydromagnetic Stability*, Dover.

Chen, H. & Montgomery, D. 1987 *Plasma Phys. Controlled Fusion* **29**, 205.

Clever, R. M. & Busse, F. H. 1974 *J. Fluid Mech.* **65**, 625.

Curry, J. H., Herring, J. R., Loncaric, J. & Orszag, S. A. 1984 *J. Fluid Mech.* **147**, 1.

Dobrowolny, M., Mangeney, A. & Veltri, P. L. 1980 *Phys. Rev. Lett.* **47**, 1060.

Frisch, U., Pouquet, A., Leorat, J. & Mazure, A. 1975 *J. Fluid Mech.* **68**, 769.

Frisch, U., Pouquet, A., Sulem, P. L. & Meneguzzi, M. 1983 *J. Méc. Theor. Appl.* **2D**, 191.

Galloway, D. & Frisch, U. 1986 *Geophys. Astrophys. Fluid Dyn.*, **36**, 53.

Gilbert, A., Frisch, U. & Pouquet, A. 1988 *Geophys. Astrophys. Fluid. Dyn*, **42**, 151.

Gilman, P. A. 1983 *Astrophy. J. Suppl.* **53**, 243.

Gilman, P. A. & Miller, J. 1981 *Astrophys. J. Suppl.* **46**, 211.

Glatzmaier, G. A. 1984 *J. Comp. Phys.* **55**, 461.

Glatzmaier, G. A. & Gilman, P. A. 1982 *Astrophys. J.* **256**, 316.

Gottlieb, D. & Orszag, S. A. 1977 *Numerical Analysis of Spectral Methods*. SIAM.

Grappin, R. 1986 *Phys. Fluids* **29**, 2433.

Grappin, R., Leorat, J. & Pouquet, A. 1983 *Astron. Astrophys.* **126**, 51.

Kraichnan, R. H. 1976 *J. Fluid Mech* **77**, 753.

Kraichnan, R. H. & Nagarajan, S. 1967 *Phys. Fluids* **10**, 859.

Kirko, I. M., Kirko, G. E., Telitchko, M. T. & Cheinkman, A G. 1982 *Proc. USSR Sci. Acad.* **266**, 1384.

Leorat, J., Pouquet, A. & Frisch, U. 1981 *J. Fluid Mech.* **104**, 419. (Paper I herein.)

Matthaeus, W. H., Goldstein, M. L. & Lantz, S. R. 1986 *Phys. Fluids* **29**, 1504.

Matthaeus, W. H., Goldstein, M. L. & Montgomery, D. 1983 *Phys. Rev. Lett.* **51**, 1484.

Matthaeus, W. H. & Montgomery, D. 1980 *Ann. NY Acad. Sci.* **357**, 203.

Matthaeus, W. H. & Montgomery, D. 1984 In *Statistical Physics and Chaos in Fusion Plasmas* (ed. C. W. Horton & L. E. Reichl), p. 285. Wiley.

Meneguzzi, M., Frisch, U. & Pouquet, A. 1981 *Phys. Rev. Lett.* **47**, 1060. (Paper II herein.)

Meneguzzi, M., Sulem, C., Sulem, P. L. & Thual, O. 1987 *J. Fluid Mech.* **182**, 169.

Moffat, H. K. 1972 *J. Fluid Mech.* **53**, 385.

Moffatt, H. K. 1978 *Magnetic Field Generation in Electrically Conducting Fluids*. Cambridge University Press.

Montgomery, D. & Hatori, T. 1984 *Plasma Phys. Controlled Fusion* **26**, 717.

Moore D. & Weiss, N. O. 1973 *J. Fluid Mech.* **58**, 289.

Parker, E. N. 1979 *Cosmical Magnetic Fields*. Clarendon Press.

Patterson, S. & Orszag, S. A. 1971 *Phys. Fluids* **14**, 2538.

Pouquet, A., Frisch, U. & Leorat, J. 1976 *J. Fluid Mech.* **77**, 321.

Pouquet, A., Meneguzzi, M. & Frisch, U. 1986 *Phys. Rev.* **A33**, 4266.

Pouquet, A. & Patterson, G. S. 1978 *J. Fluid Mech.* **85**, 305.

Schlüter, V. A. & Biermann, L. 1950 *Z. Naturforsch.* **5A**, 237.

Shtilman, L., Levitch, E., Orszag, S. A., Peltz, R. B. & Tsinober, A. 1985 *Phys. Lett.* **113A**, 32.

Smith, C. W., Matthaeus, W. H. & Goldstein, M. L. 1983 *J. Geophys. Res.* **88**, 5581.

Soward, A. M. 1974 *Phil. Trans. R. Soc. Lond.* A **275**, 611.

Spiegel, E. 1971 *Ann. Rev. Astron. Astrophys.* **9**, 323.

Steenbeck, M., Krause, F. & Radler, K. H. 1966 *Z. Naturforsch.* **21**, 369.

Ting, A., Matthaeus, W. H. & Montgomery, D. 1986 *Phys. Fluids* **29**, 3261.

Yakhot, V., Orszag, S. A., Yakhot, A., Frisch, U. & Kraichnan, R. H. 1987 in press.

Zeldovich, Y. B., Ruzmaikin, A. A. & Sokolov, D. D. 1983 *Magnetic Fields in Astrophysics*, vol. 3, p. 191. Gordon & Breach.